Development 125, 825-836 (1998)
Printed in Great Britain © The Company of Biologists Limited 1998
DEV9582

Dual genetic pathways of endothelin-mediated intercellular signaling revealed by targeted disruption of endothelin converting enzyme-1 gene

Hiromi Yanagisawa[2], Masashi Yanagisawa[1,3,†], Raj P. Kapur[5], James A. Richardson[4], S. Clay Williams[1,3], David E. Clouthier[1,3], Damiane de Wit[1,3], Noriaki Emoto[1,3,*] and Robert E. Hammer[1,2]

[1]Howard Hughes Medical Institute, [2]Department of Biochemistry, [3]Department of Molecular Genetics, [4]Department of Pathology, The University of Texas Southwestern Medical Center at Dallas, 5323 Harry Hines Boulevard, Dallas, Texas 75235-9050, USA
[5]Department of Pathology, University of Washington Medical Center, Seattle, Washington 98195, USA
*Present address: International Center for Medical Research, Kobe University School of Medicine, Kobe 650, Japan
†Author for correspondence (e-mail: afcsushi@aol.com)

Accepted 8 December 1998: published on WWW 4 February 1998

SUMMARY

Recent gene targeting studies have revealed unexpected roles for endothelins in the development of neural crest-derived tissues. Endothelin converting enzyme-1 (ECE-1) catalyzes the proteolytic activation of big endothelin-1 to endothelin-1(ET-1) in vitro. However, the importance of ECE-1 cleavage in the multiple endothelin pathways in vivo is unknown. Here we generated a targeted null mutation in the mouse *ECE-1* gene. *ECE-1*$^{-/-}$ term embryos exhibited craniofacial and cardiac abnormalities virtually identical to the defects seen in *ET-1* and endothelin A receptor (*ET*$_A$)-deficient embryos. Epidermal melanocytes as well as enteric neurons of the distal gut were also absent in *ECE-1*$^{-/-}$ embryos, reproducing the developmental phenotype seen in *ET-3*$^{-/-}$ and endothelin B receptor *(ET*$_B$*)*$^{-/-}$ mice. Surprisingly, large amounts of mature ET-1 peptide are found in *ECE-1*$^{-/-}$ embryos, indicating that non-ECE-1 protease(s) can activate ET-1 at certain sites. However, these enzymes cannot produce sufficient mature endothelin at the locations crucial for normal embryonic development. These findings reveal that ECE-1 is a bona fide activating protease for both big ET-1 and big ET-3 in vivo, and that the cell-cell communication pathways represented by the ET-1/ECE-1/ET$_A$ axis and the ET-3/ECE-1/ET$_B$ axis are each involved in the development of distinct subsets of neural crest cell lineages. Mutations in ECE-1 may cause developmental defects in humans, such as Hirschsprung disease, velocardiofacial syndrome and related neurocristopathies.

Key words: Mouse, Neural crest, Heart, Branchial arch, Melanocyte, Enteric neuron, Protease, ECE-1

INTRODUCTION

Neural crest cells arise at the dorsal aspect of the neural tube between the neural plate and surface ectoderm, and migrate extensively along the dorsoventral axis as the neural tube fuses. The fate and final derivatives of neural crest cells have been analyzed in quail-chick chimeras (Le Douarin et al., 1993) and neural crest-ablated chick embryos (Kirby et al., 1983). In addition, direct labeling of premigratory and migratory neural crest cells with lineage tracers such as fluorescent marker molecules and replication-defective retroviruses (Serbedzija et al., 1992; Epstein et al., 1994; Noden et al., 1995) have provided the information regarding the spatiotemporal pattern of neural crest cell migration in vivo. The neural crest can be divided into four partially overlapping groups according to the neural axis from which they emigrate, i.e., cephalic, cardiac, vagal and trunk neural crests. Cephalic neural crest gives rise to the connective tissues of the head and neck, cranial ganglia, and mesenchyme of the arch arteries (Le Lièvre and Le Douarin, 1975). In mice, the cephalic neural crest has three main streams of cells that emigrate from the level of forebrain, midbrain and hindbrain. At the level of the rostral hindbrain, cephalic neural crest cells migrate along a dorsolateral pathway to populate the first, second and third branchial arches (Serbedzija et al., 1992). Neural crest cells originating from the level of the otic placode to somite 3 are called cardiac neural crest. They migrate to the third, fourth and sixth branchial arches and further proceed to the conotruncal region of the heart (Kuratani and Kirby, 1991). Vagal neural crest consists of cells originating from the somite levels 1-7. These cells migrate ventromedially to enter the mesenchyme of the foregut and differentiate into enteric neuroblasts, which proceed caudally to eventually colonize the entire length of the gut (Durbec et al., 1996). Finally, trunk neural crest cells migrate subectodermally to give rise to melanocytes in the skin, and ventromedially to form sensory and sympathetic neurons, adrenomedullary cells and Schwann cells (Loring and Erickson, 1987; Erickson, 1993).

The unique characteristics of neural crest cells have made them a valuable tool to study the molecular mechanisms of lineage determination (Shah et al., 1996), epithelial-mesenchymal transformation (Trainor and Tam, 1995), cell-

cell interaction during migration (Serbedzija and McMahon, 1997) and cell diversification in a final environment (Stemple and Anderson, 1993; Le Douarin et al., 1994). Recent gene inactivation studies in mice have elucidated several signaling pathways involved in neural crest development. They have enabled us to relate the phenotype resulting from the defect of a gene to a specific human disease. Several components of the endothelin (ET) system have been inactivated in mice by homologous recombination, and have unexpectedly shown that endothelin-mediated cell-cell signaling is essential for the development of the subsets of neural crest lineages (Baynash et al., 1994; Hosoda et al., 1994; Kurihara et al., 1994; Clouthier et al., 1998). The endothelins are a family of small 21-amino-acid peptides composed of three structurally related isoforms called ET-1, ET-2 and ET-3 (Inoue et al., 1989). They act on two distinct receptors, the endothelin-A receptor (ET_A) and the endothelin-B receptor (ET_B), both of which belong to the seven membrane-spanning G protein-coupled receptor family (Arai et al., 1990; Sakurai et al., 1990). ET_A can bind ET-1 and ET-2 but not ET-3 at physiological concentrations, whereas ET_B accepts all three ligands with equal high affinity. Mice deficient in *ET-1* have defects in craniofacial structures and the conotruncal region, suggesting deficits in the cephalic and cardiac neural crest (Kurihara et al., 1994, 1995). Our recent finding that mice deficient in ET_A exhibited virtually identical craniofacial and cardiovascular abnormalities to that of *ET-1*-deficient mice demonstrates that ET-1/ET_A-mediated paracrine signaling is essential for the development of subsets of cephalic neural crest-derived tissues (Clouthier et al., 1998). In contrast, mice deficient in *ET-3* or ET_B each develop spotted coat color and aganglionic megacolon resulting from the absence of epidermal melanocytes and enteric neurons (Baynash et al., 1994; Hosoda et al., 1994). The mutations of *ET-3* and ET_B were also reported in patients of both sporadic and familial Hirschsprung disease with or without pigmentary abnormalities (Puffenberger et al., 1994; Edery et al., 1996; Hofstra et al., 1996), underscoring the importance of ET-3/ET_B-mediated signaling in development of enteric neurons and melanocytes in humans.

The biosynthesis of endothelins occurs through two steps of proteolytic processing resulting in the production of biologically active peptides. Approximately 200-residue preproendothelins are first processed by a furin-like processing protease into biologically inactive intermediates called big endothelins. They are then proteolytically activated via cleavage at the common Trp21 residue by the highly specific endothelin converting enzymes (ECEs). Two isozymes of ECE (ECE-1 and ECE-2) have been molecularly identified and each shown to belong to the type II membrane-bound metalloprotease family (Xu et al., 1994; Emoto and Yanagisawa, 1995). In vitro, both ECE-1 and ECE-2 catalyze the conversion of big ET-1 to ET-1 most efficiently among the three isopeptides. Production of active endothelins is thought to be regulated at the level of these converting enzymes as well as at the level of transcription of prepropeptide mRNAs. However, the importance of ECE-1 and ECE-2 activity in neural crest development is unknown. In this study, we report the generation of a targeted null mutation in the mouse *ECE-1* gene, which reveals dual genetic pathways of endothelin-mediated signaling, each involved in the development of distinct subsets of neural crest cell lineages.

MATERIALS AND METHODS

Mice

Mice deficient for ET_A and ET_B were generated by gene targeting as described (Hosoda et al., 1994; Clouthier et al., 1998) and maintained on a 129SvEv background in our animal facilities. Dopamine-β-hydroxylase (*DβH*)-*nlacZ* transgenic mice were generated and maintained as previously described (Kapur et al., 1991).

Targeting vector

To isolate the mouse *ECE-1* genomic fragment, we screened a λFIX II mouse 129/Sv genomic library (Stratagene Inc.) with a 92-bp RT-PCR product previously described (Xu et al., 1994). Two phage clones encompassing a 17 kb DNA fragment containing the catalytic domain of ECE-1 were isolated. To construct the targeting vector, we used a universal *neo-TK* template plasmid vector that contained a *neo*^{r} gene and two tandem *TK* cassettes (Hosoda et al., 1994). A 5′ homologous 4.5 kb *Sac*I fragment was blunt-end inserted into the unique *Xho*I site of the plasmid between the *neo*^{r} and *TK* cassettes. A 3′ homologous 10.5 kb *Sal*I fragment of the *ECE-1* gene was then blunt-end inserted into the unique *Bam*HI site of the plasmid. The exon immediately 5′ to the one encoding the zinc-binding domain of *ECE-1* was replaced with a *neo*^{r} cassette as shown in Fig. 2A.

Generation of mice with targeted allele

SM-1 ES cells were cultured on an irradiated LIF-producing STO feeder layer (gift from A. Bradley) as previously described (Ishibashi et al., 1993). ES cells were transfected with a linearized targeting vector by electroporation (BRL Cell Porator) at 275 V, 330 μF and selected in 190 μg/ml G418 (Gibco-BRL) and 79 μg/ml FIAU (1-(2′-deoxy-2′-fluoro-β-D-arabinofuranosyl)-5-iodouracil, gift from Bristol Myers-Squibb). Double resistant ES cell clones were isolated and homologous recombination was confirmed by Southern blot analysis of *Apa*I-*Bam*HI-digested genomic DNA hybridized with the 5′ external probe described in Fig. 2A. *Eco*RI-digested genomic DNA was also hybridized with a *neo* probe (data not shown). Five ES cell clones were established and injected into blastocysts obtained from C57BL/6 female mice, and resulting chimeric males were bred to C57BL/6 females to produce heterozygous F_1 mice carrying the targeted allele. Original chimeras were bred to 129SvEv females to obtain heterozygous mice on a 129SvEv background.

Genotyping

Genomic DNA was prepared from tail biopsies from postnatal day 21 mice or yolk sac from embryos, and subjected to polymerase chain reaction (PCR) and/or Southern blot analysis. Oligonucleotide primers used for the detection of the wild-type *ECE-1* allele were upstream, 5′-ATGACGCCGCCCATGGTGAAC-3′ and downstream, 5′-TGGTTGGGCTAAGACATAAC-3′. Primers used for the detection of *neo*^{r} were upstream, 5′-TATTCGGCTATGACTGGGCACAACAG-3′ and downstream, 5′-TTCCACCATGATATTCGGCAAGCAGG-3′. The reaction was cycled 30 times (30 seconds at 94°C, 1 minute at 60°C, 3 minutes at 72°C), which amplified a 128 bp fragment of the deleted *ECE-1* gene and a 500 bp fragment of the *neo*^{r} gene, respectively. For Southern blot analysis, 10 μg of genomic DNA was digested with *Apa*I and *Bam*HI and hybridized with the 5′ external probe as described above.

Membrane preparations and immunoblotting

E18.5 embryos were minced in a 10× volume of homogenization buffer (20 mM Tris-HCl (pH 7.4), 10 μM pepstatin A, 1 mM PMSF, 1 mM pCMS, 250 mM sucrose) and then homogenized using a 30 ml Teflon homogenizer with piston rotation at 400 revs/minute. Homogenates were centrifuged at 1,000 ***g*** for 10 minutes, and the resulting supernatant was further centrifuged at 100,000 ***g*** for 60 minutes. The pellet was resuspended in a 5× volume of

homogenization buffer using a Teflon homogenizer and centrifuged again at 100,000 ***g*** for 60 minutes. The pellet was resuspended in a 1× volume of homogenization buffer, aliquoted and protein concentrations were determined by the Bradford method (Bio-Rad) using IgG as standard. 100 μg of each membrane protein was subjected to SDS-PAGE and filters were probed with an antibody against the C terminus of bovine ECE-1 (Emoto and Yanagisawa, 1995) and developed using the ECL kit (Amersham) as recommended by the manufacturer.

ECE-1 enzyme assay

Membrane fractions from E18.5 embryos (10-40 μg protein) were incubated with 0.1 μM human big ET-1 (1-38) (American Peptides) in 0.1 M sodium phosphate buffer (pH 6.8), 0.5 M NaCl at 37°C for 30 minutes. Enzyme reactions were terminated by adding 2.5 mM EDTA and mature ET-1 (1-21) production measured by EIA (Suzuki et al., 1990). Duplicate assay wells were used for each enzyme reaction. For the enzyme inhibition assay, 40 μg of membrane protein were incubated with 0.1 μM human big ET-1 (1-38) with or without 100 μM phosphoramidon (Sigma).

Peptide measurement

Near-term whole embryos were homogenized using a Polytron (20,000 revs/minute) in 1 M acetic acid containing 0.01 mM pepstatin A for 1 minute, and immediately placed in boiling water for 10 minutes. After centrifugation at 25,000 ***g***, supernatant was concentrated with Sep-Pak C18 columns (Varian) as previously described (Matsumoto et al., 1989). Mature ET-1/ET-2, big ET-1, mature ET-3 and big ET-3 were separately determined by EIA as previously described (Baynash et al., 1994; Xu et al., 1994).

General histology and skeletal preparation

Embryos were harvested at E18.5 and fixed overnight in 10% neutral buffered formalin (NBF) with gentle shaking. Samples were then dehydrated in a series of ethanols, followed by xylene and then embedded in paraffin. Sections were cut at 4 μm and stained with hematoxylin and eosin. For skeletal preparations, skin and viscera were removed from freshly harvested embryos. The embryos were fixed and stained in alcian blue 8GX (Sigma) and alizarin red S (Sigma) as previously described (Kochhar, 1973).

L-DOPA histochemistry and immunohistochemistry

To examine the choroidal melanocytes, 10 μm cryosections of the head from P0 mice were fixed in 10% NBF at room temperature for 10 minutes and stained with methyl green (Zymed). For visualization of skin melanocytes, 10 μm parasagittal cryosections of the lower body from P0 mice were paraformaldehyde-fixed and subjected to L-DOPA reaction as previously described (Rodriguez and McGavran, 1969). For anti-peripherin immunostaining, 4 μm paraffin sections from E18.5 embryos were used. Sections were first microwaved in 10 mM citrate buffer for 12 minutes to unmask antigens, and then treated with 0.01% pronase followed by 0.6% H_2O_2 to quench endogenous peroxidases. Sections were incubated with an anti-peripherin antibody (1:1,000, Chemicon) at room temperature for 90 minutes, followed by a biotinylated goat anti-rabbit antibody (ABC kit, Vector Laboratories) at room temperature for 30 minutes. The chromogen diaminobenzidine was used for signal detection.

Whole-gastrointestinal tract X-gal staining

Mice homozygous for the *DβH-nlacZ* transgene were bred to *ECE-1* heterozygous mice to subsequently generate male mice homozygous for the transgene and heterozygous for *ECE-1*. These were then bred to *ECE-1* heterozygous females to obtain embryos that were positive for the transgene and wild type, heterozygous or homozygous for the targeted *ECE-1* allele. The morning that the vaginal plug was found was counted as 0.5 d.p.c. Pregnant females were killed on 12.0 d.p.c. by inhalation of CO_2 and embryos harvested from the uterus. Gastrointestinal tracts of E12.0 embryos were isolated and fixed for 1 hour in 10% NBF, rinsed with 0.1 M phosphate buffer (pH 7.4) and stained overnight at 37°C in a buffer containing 1 mg/ml X-gal substrate, 5 mM $K_3Fe(CN)_6$ and 5 mM $K_4Fe(CN)_6$. Stained gastrointestinal tracts were postfixed for 24 hours in 10% NBF.

In situ hybridization

Sectional in situ hybridization analysis was performed as described previously (Benjamin et al., 1997) except that riboprobes were labeled with both ^{35}S-CTP and ^{35}S-UTP (>1,000 Ci/mmol, Amersham) using the Maxiscript In Vitro Translation Kit (Ambion). To make the RNA probes, a 350 base pair *Eco*RV-*Bam*HI fragment from the mouse ET_A cDNA was subcloned into pBluescript SK+. The resulting plasmid was digested with *Eco*RV and transcribed with T7 RNA polymerase (anti-sense), or digested with *Bam*HI and transcribed with T3 RNA polymerase (sense). For the *ECE-1* probe, a 350 base pair *Eco*RI fragment from the mouse *ECE-1* cDNA was subcloned into pBluescript SK+. The resulting plasmid was digested with *Xba*I and transcribed with T7 RNA polymerase (antisense) or digested with *Xba*I and transcribed with T3 RNA polymerase (sense).

RESULTS

Expression of *ECE-1* mRNA in embryos

The phenotype observed in $ET\text{-}1^{-/-}$ (Kurihara et al., 1994) or $ET_A^{-/-}$ (Clouthier et al., 1998) embryos do not overlap that in $ET\text{-}3^{-/-}$ (Baynash et al., 1994) or $ET_B^{-/-}$ (Hosoda et al., 1994) mice, indicating that cell populations affected in $ET\text{-}1^{-/-}$ or $ET_A^{-/-}$ embryos are different from those in $ET\text{-}3^{-/-}$ or $ET_B^{-/-}$ mice. We have also examined the expression of ligand (ET-1, ET-3) and receptor (ET_A, ET_B) mRNA in wild-type mouse embryos and found that ET-1/ET_A and ET-3/ET_B mRNA were expressed in a complementary fashion in adjacent cell types (R. P. Kapur et al., unpublished data; Clouthier et al., 1998, see Fig. 8A). Thus, ET_A and ET_B receptors are expressed in specific neural crest-derived cells, while ET-1 and ET-3 ligands are made by surrounding cells. These observations suggested that two endothelin-mediated signaling pathways (ET-1/ET_A and ET-3/ET_B) are independently acting on the different subsets of neural crest lineages in a paracrine manner. To determine whether ECE-1 qualifies as a relevant converting enzyme in these developmental processes, we examined the expression of *ECE-1* mRNA in wild-type mouse embryos by in situ hybridization analysis and compared it with localization of the ligands and receptors. In E9.5 embryos, *ECE-1* mRNA is strongly expressed in head mesenchyme adjacent to the neuroepithelium, liver primordia, heart and gut (Fig. 1A). *ECE-1* is also expressed in parts of the neuroepithelium, although the phenotypic significance of this is unclear. In the branchial arch, *ECE-1* mRNA is expressed in both the mesenchyme and surface epithelium (Fig. 1B). In addition, *ET-1* mRNA is expressed in the surface epithelium of arches 1, 2 and 3 and associated endodermal pouches (Maemura et al., 1996; Clouthier et al., 1998). It is also observed in the paraxial mesoderm core of arches 1 and 2. In contrast, ET_A mRNA is expressed in migrating neural crest cells of the head, as well as in the ecto-mesenchyme of arches 1, 2 and 3. In developing heart, *ECE-1* expression is seen in the endocardial layers of ventricle, atrium and cushions (Fig. 1C). In contrast, ET_A mRNA is found in the myocardium (Fig. 1D), while ET_B mRNA co-localized with *ECE-1* mRNA in the embryonic heart

(R. P. Kapur et al., unpublished data). In the developing gastrointestinal tract, *ECE-1* expression is observed in the mesenchyme of the foregut at E9.5 (Fig. 1E). *ET-3* expression is also seen in the mesenchyme of the foregut from E9.0, which is before neuroblasts migrate into the gut. In contrast, ET_B mRNA is expressed in premigratory and migratory neural crest, and later in enteric neuroblasts (R. P. Kapur et al., unpublished data). In the skin, *ECE-1* mRNA is expressed in dermal mesenchyme (Fig. 1F) where *ET-3* expression is also detected, while ET_B expression is seen in migrating melanoblasts. Taken together, ECE-1 is expressed at the site of ET-1 and ET-3 production in mouse embryos. These observations are compatible with the idea that ECE-1 is a relevant activating enzyme that cleaves big ET-1 and big ET-3 in vivo.

Generation and biochemical characterization of *ECE-1* null mice

ECE-1 is a type II integral membrane protein, which possesses a short cytoplasmic tail in the N-terminus followed by a membrane spanning region and a large extracellular catalytic domain. The extracellular domain contains a zinc-binding motif, ϕXHEϕϕHϕΨ (ϕ and Ψ denotes uncharged and hydrophobic amino acid residues, respectively), which is essential for enzymatic activity (Rawlings and Barrett, 1993). To inactivate *ECE-1* in vivo, the exon immediately 5′ to the one encoding the zinc-binding motif was replaced with the *neo*^{r} gene by homologous recombination (Fig. 2A). The targeting vector was electroporated into ES cells, and transfected cells were doubly selected in the presence of G418 and FIAU. Surviving colonies were individually picked and the homologous recombination event was confirmed by genomic Southern blot analysis (data not shown). Recombinant ES cell clones were injected into blastocysts obtained from C57BL/6 females and resulting male chimeras were bred to C57BL/6 females to verify germline transmission. Four chimeras from three independent ES cell clones gave germline transmission. There was no phenotypic difference between each line of mice. Heterozygous *ECE-1*$^{+/-}$ mice were healthy and fertile, and had the same life span as wild-type littermates. *ECE-1*$^{+/-}$ mice were then intercrossed to generate homozygous *ECE-1*$^{-/-}$ mice (Fig. 2B).

Western blot analysis was performed using membrane preparations from E17-19 whole embryos. In *ECE-1*$^{+/-}$ mice, the intensity of the 126 kDa band corresponding to ECE-1 protein was significantly decreased compared with that of wild-type embryos. In *ECE-1*$^{-/-}$ embryos, this band was absent (Fig. 2C). An ECE-1 enzyme assay was performed by incubating the synthetic human big ET-1 with the membrane preparations from near-term whole embryos, followed by determination of mature ET-1 production by enzyme immunoassay. It showed that ECE-1 activity was undetectable in *ECE-1*$^{-/-}$ embryos (Fig. 3A). In *ECE-1*$^{+/-}$ mice, ≈73% of enzyme activity remained and this was completely inhibited by 100 μM phosphoramidon, an ECE inhibitor, indicating that the disrupted activity reflects authentic ECE-1 (Fig. 3B). These results confirmed that the targeted *ECE-1* allele was functionally null.

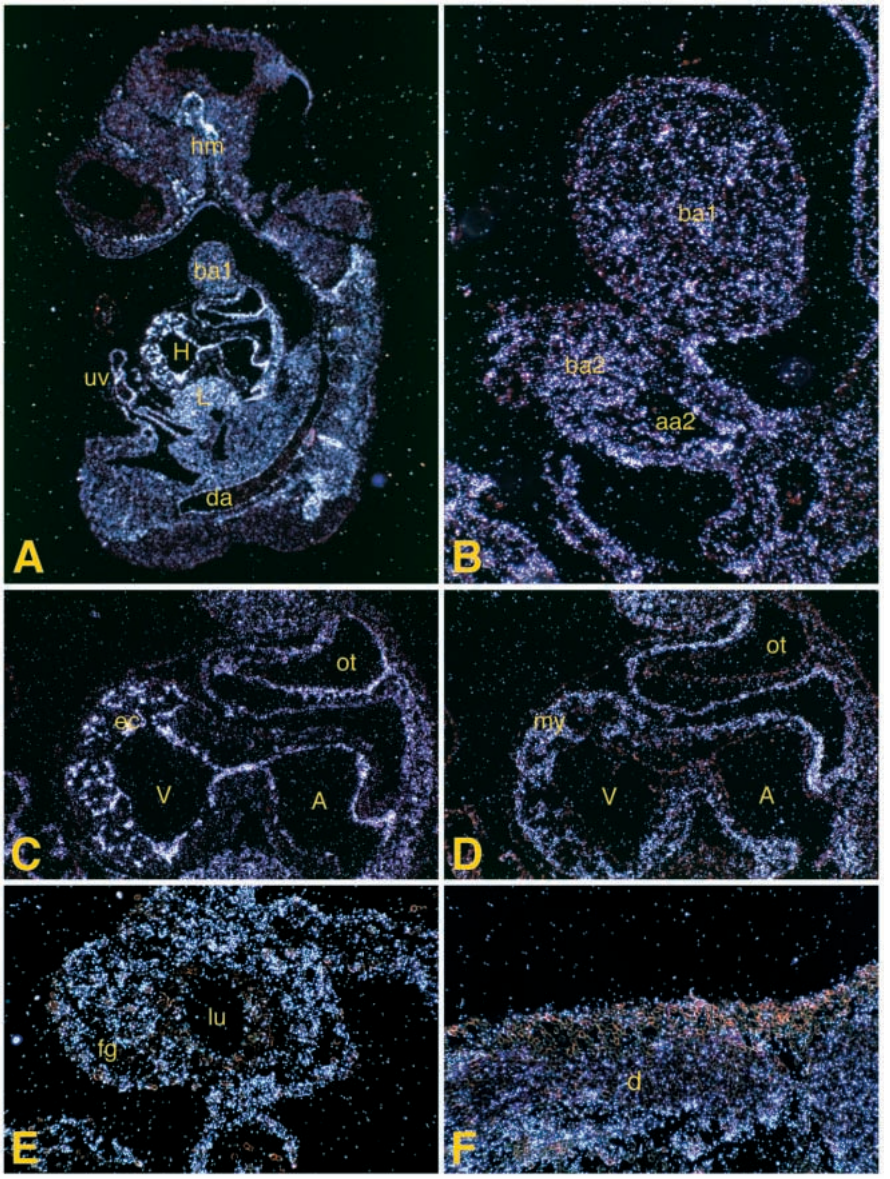

Fig. 1. Expression of *ECE-1* (A-C,E,F) and ET_A mRNA (D) in wild-type mouse embryos at E9.5 (A-E) and E11.5 (F) (parasagittal sections). (B) *ECE-1* mRNA in surface epithelium and mesenchyme of the first and second branchial arches (ba1, ba2). (C) *ECE-1* mRNA in endocardium (ec) of the ventricle (V), atrium (A) and outflow tract (ot) of the heart. (D) ET_A mRNA in myocardium (my) of the heart and neural crest-derived mesenchyme of the outflow tract. (E) *ECE-1* mRNA in mesenchyme of the foregut (fg). (F) *ECE-1* mRNA in the dermal mesenchyme (d). aa2, second branchial arch artery; da, dorsal aorta; H, heart; hm, head mesenchyme; L, liver; lu, lumen of foregut; uv, umbilical vessel.

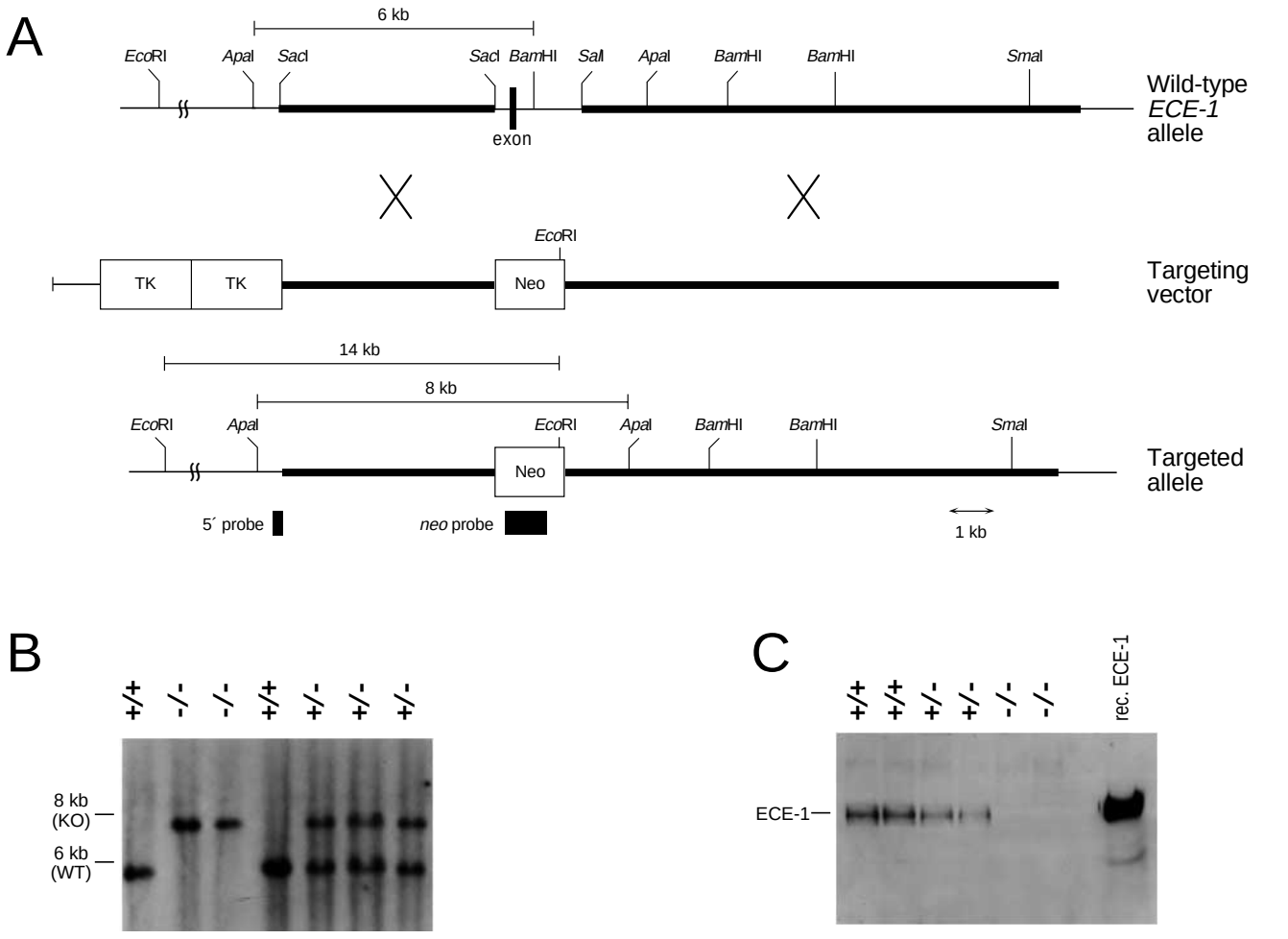

Fig. 2. Generation of *ECE-1*$^{-/-}$ embryos. (A) Targeting strategy. The exon immediately 5′ to the one encoding the zinc-binding domain of *ECE-1* is replaced with a *neo*^{r} cassette driven by the RNA polymerase II promoter. (B) Southern blot analysis of tail DNA obtained from *ECE-1* heterozygous crosses. DNA is digested with *Apa*I and *Bam*HI, and hybridized with the 5′ external probe shown in Fig. 2A. KO, targeted allele; WT, wild-type allele. (C) Western blot analysis of ECE-1 protein in membrane fractions from E18.5 whole embryos. Recombinant ECE-1 is used as a marker (rec. ECE-1).

Tissue endothelin levels in *ECE-1* null mice

We determined the levels of big and mature endothelins in E17-19 whole embryo homogenates by enzyme immunoassay (Fig. 3C). There was no significant difference in the levels of mature endothelins between *ECE-1*$^{+/+}$ and *ECE-1*$^{+/-}$ embryos, suggesting that *ECE-1*$^{+/-}$ embryos can compensate for the production of mature endothelins despite the reduction of ECE-1 activity. ET-3 levels in *ECE-1*$^{-/-}$ embryos were markedly decreased compared with those in *ECE-1*$^{+/-}$ or *ECE-1*$^{+/+}$ embryos, although the levels were still higher than those in *ET-3*$^{-/-}$ embryos in which ET-3 was undetectable (<0.8 fmol/g tissue; data not shown) (Baynash et al., 1994). Surprisingly, however, the combined level of ET-1 and ET-2 in *ECE-1*$^{-/-}$ embryos was decreased by only 48% as compared to wild-type embryos, despite the absence of detectable ECE-1 activity. There was no significant difference in levels of big ET-1 and big ET-3 among the genotypes (data not shown), indicating that big endothelins, which are not correctly processed due to the absence of ECE-1, are degraded into non-immunoreactive entities.

A majority of *ECE-1* null embryos die in utero

Embryos obtained by near-term Cesarean sections from heterozygous intercrosses consisted of 29.5% *ECE-1*$^{+/+}$ (66/224), 63.4% *ECE-1*$^{+/-}$ (142/224) and 7.1% *ECE-1*$^{-/-}$ (16/224), indicating ≈75% embryonic lethality in a C57BL/6–129SvEv hybrid background. Genotyping of earlier embryos showed a gradual decrease in the number of viable homozygous embryos starting E12.5 (data not shown). On a 129SvEv background, all homozygous embryos died before E13.5, indicating an effect of genetic background on embryonic lethality. Premorbid *ECE-1*$^{-/-}$ embryos exhibited peripheral vascular dilatation (Fig. 4B) and pericardial effusion, consistent with cardiac failure. Histological examination showed marked congestion and dilatation of the atria and peripheral vessels, as well as generalized edema (Fig. 4D). The endocardial cushion was poorly developed in *ECE-1*$^{-/-}$ embryos, suggesting probable malfunction of the atrioventricular valves. The embryonic lethal phenotype is not observed in *ET-1*$^{-/-}$ (Kurihara et al., 1994), *ET-2*$^{-/-}$ (our unpublished data), *ET-3*$^{-/-}$ (Baynash et al., 1994), *ET*$_A$$^{-/-}$

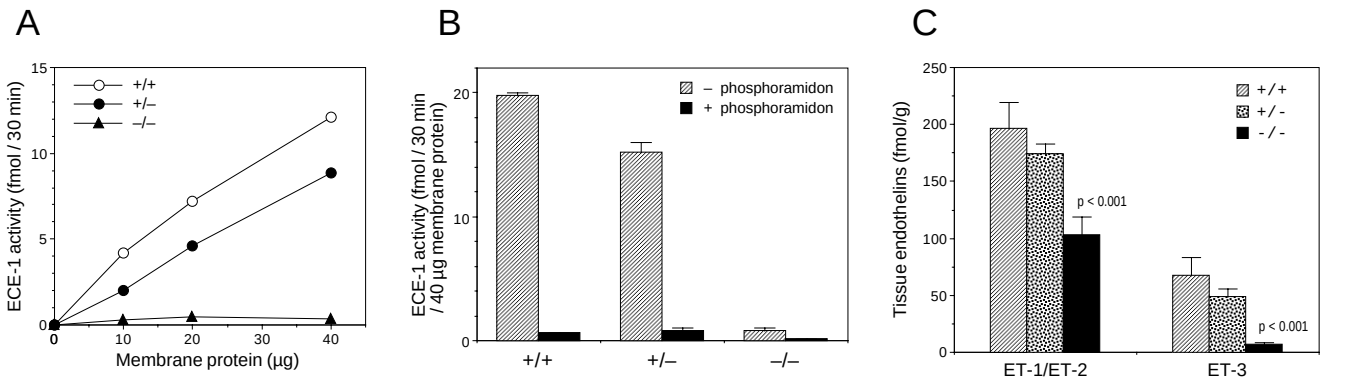

Fig. 3. Biochemical characterization of *ECE-1*$^{-/-}$ embryos. (A) ECE-1 enzyme assay in near-term embryos (n=4). (B) Inhibition of ECE-1 activity by phosphoramidon. Values are means ± s.e.m. (n=4). (C) ET-1/ET-2 and ET-3 peptide levels in near-term whole embryos (+/+, n=6; +/–, n=3; –/–, n=6). Values are means ± s.e.m. Statistical analysis by ANOVA.

(Clouthier et al., 1998), *ET$_B$*$^{-/-}$ (Hosoda et al., 1994) or *ECE-2*$^{-/-}$ (our unpublished data) mice, and it is clearly more profound than the phenotype that results from the disturbance of either the ET-1/ET$_A$- or ET-3/ET$_B$-mediated pathway alone.

Craniofacial and cardiovascular abnormalities in *ECE-1* null mice

Homozygous *ECE-1*$^{-/-}$ mice that survived to term all died within 30 minutes of birth, apparently from impaired breathing. Strikingly, they showed gross malformations identical to *ET-1*$^{-/-}$ (Kurihara et al., 1994) and *ET$_A$*$^{-/-}$ mice (Clouthier et al., 1998) (Fig. 5A). They were cyanotic and had a hypoplastic jaw, pinnae and sunken ventral neck. Skeletal preparations of *ECE-1*$^{-/-}$ embryos showed marked reduction of the mandibular bone and absence of the tympanic ring (Fig. 5C). Meckel's cartilage was also absent, and the palatine bone and constituents of the temporal skull including alisphenoid and squamosal bones were hypoplastic and deformed. The fusion of the thyroid cartilage, hyoid bone and basisphenoid bone narrowed the upper airway in a manner similar to that of *ET$_A$*$^{-/-}$ and *ET-1*$^{-/-}$ mice (Fig. 5C,G). Histological analysis showed that most of the tongue as well as submandibular and sublingual ducts were absent from homozygous embryos (Fig. 5E). Teeth were intact, although the lower incisors were embedded in loose mesenchyme instead of mandibular bone. The thyroid and parathyroid glands were hypoplastic and the thymus did not completely descend into the thoracic cavity. The external auditory meatus, malleus and incus were absent and the stapes and styloid process were often severely deformed, although inner ear structure appeared normal (not shown). The penetrance of these craniofacial defects was 100%. Cranial ganglia V, VII, VIII, IX and X were all present in term *ECE-1*$^{-/-}$ embryos, as well as in E10.5 *ECE-1*$^{-/-}$ embryos examined through continuous histological sections. Further, the size and positions of these cranial ganglia in *ECE-1*$^{-/-}$ embryos appeared the same as those of wild-type embryos. While we did not examine the development of the cranial nerves projecting from the ganglia, it is likely that their development is affected in their distal branches, based on the findings observed in *ET$_A$*$^{-/-}$ embryos (Clouthier et al., 1998).

We also observed various malformations in both the cardiac conotruncal region and great vessels in *ECE-1*$^{-/-}$ embryos, suggesting defects in cellular interactions involving the cardiac neural crest (Kirby and Waldo, 1995). Most common was the interruption or tubular hypoplasia of the aortic arch between the left common carotid artery and the left subclavian artery (58% penetrance, 18/31, Fig. 6B,C, respectively). We also observed absent right subclavian artery (23%, 7/31, Fig. 6C), right-sided aortic arch (16%, 5/31, Fig. 6D) and double aortic

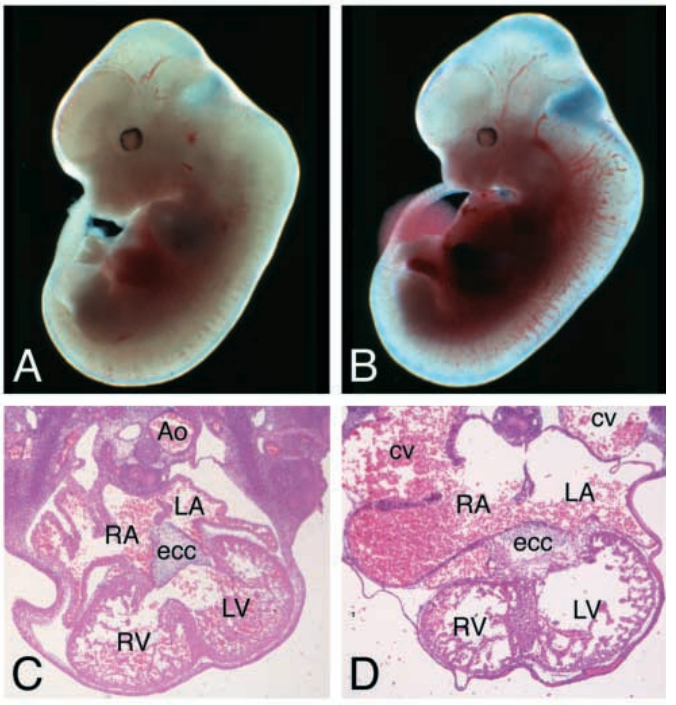

Fig. 4. Gross photographs of E12.5 wild-type (A) and *ECE-1*$^{-/-}$ (B) embryos. Note that the *ECE-1*$^{-/-}$ embryo shows marked dilatation of peripheral vessels and congestion of the liver. Transverse sections through the heart of E12.5 wild-type (C) and *ECE-1*$^{-/-}$ (D) embryos. The mutant embryo shows marked dilatation of atria and cardinal veins (cv). The endocardial cushion (ecc) is poorly developed compared with the wild-type embryo. Ao, aorta; LA, left atrium; LV, left ventricle; RA, right atrium; RV, right ventricle.

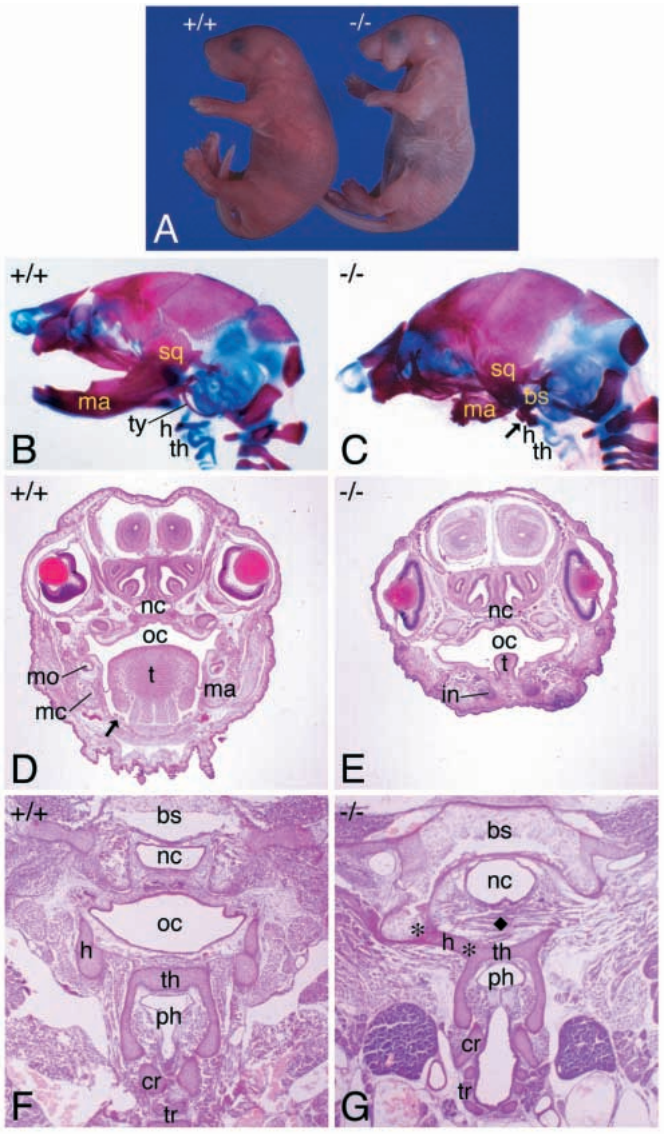

Fig. 5. Craniofacial defects in *ECE-1*$^{-/-}$ mice. (A) Gross photograph of P0 wild-type and *ECE-1*$^{-/-}$ mice. Mutant mouse (right) is cyanotic and shows hypoplastic jaw and pinna. (B,C) Skeletal preparations with alizarin red and alcian blue. (D-G) Frontal sections of the head and neck stained with hematoxylin and eosin. *ECE-1* genotype is indicated in each panel. Note hypoplastic mandible (ma) and abnormal fusion (arrow) of the hyoid (h) with basisphenoid bone (bs) and thyroid cartilage (th) in the mutant (C). (E) Lower incisors (in) are embedded in mesenchyme instead of mandible; both submandibular and sublingual ducts (arrow in D) are absent. (G) The oral cavity (oc in F) is obstructed (◆). Abnormal fusions between the basisphenoid bone, hyoid bone and thyroid cartilage are shown (*). cr, cricoid cartilage; mc, Meckel's cartilage; mo, molar; nc, nasal cavity; ph, pharynx; sq, squamosal bone; t, tongue; tr, tracheal ring; ty, tympanic ring.

arch (3%, 1/31). Histological examinations showed various conotruncal defects including perimembranous ventricular septal defect (VSD; 100%, 10/10, Fig. 6F), overriding aorta (50%, 5/10, Fig. 6F), double outlet right ventricle (DORV; 30%, 3/10) and persistent truncus arteriosus (PTA; 10%, 1/10). The cumulative incidence of cardiac abnormalities was 100% and stood in striking contrast to a much lower incidence in *ET-1*$^{-/-}$ embryos (Kurihara et al., 1995).

Enteric neurons and neural crest-derived melanocytes are absent in *ECE-1* null mice

We previously demonstrated that interaction of ET-3 with the ET_B receptor is essential for the development of epidermal melanocytes and enteric neurons (Baynash et al., 1994; Hosoda et al., 1994). We examined melanocytes and enteric neurons in *ECE-1*$^{-/-}$ embryos in order to analyze whether this genetic pathway is also affected. Since all homozygous mutants died shortly after birth due to the craniofacial defects, we were unable to evaluate the presence of epidermal melanocytes by coat color. Therefore we examined the neural crest-derived melanocytes in the choroidal layer of the eye and around the Harderian glands on frozen sections of the head of P0 homozygous mice. Pigmentation in the choroidal and Harderian gland melanocytes was clearly visible in the eye of term wild-type mice (Fig. 7A). In contrast, these neural crest-derived melanocytes were absent in *ECE-1*$^{-/-}$ mice. Only retinal pigmented epithelium, which is derived from the neural tube, was present in *ECE-1*$^{-/-}$ mice (Fig. 7B). We also performed L-DOPA histochemistry on dorsal skin of term embryos to visualize the presence of melanocytes, which were not yet fully capable of synthesizing the melanin granules in epidermis and hair follicles. In wild-type embryos, there were numerous dermal and follicular melanocytes that were positive for L-DOPA reaction (Fig. 7C). In contrast, there were no detectable melanocytes in the dorsal skin of term *ECE-1*$^{-/-}$ mice as judged by the absence of brown deposits after L-DOPA reaction (Fig. 7D).

We also examined the presence of enteric neurons in distal colon. Rectal sections of wild-type embryos clearly showed enteric neurons between the circular and longitudinal smooth muscle layers (Fig. 7E). These cells were positive for anti-peripherin immunostaining, confirming their neuronal phenotype (Fig. 7E, inset). In contrast, rectal sections of *ECE-1*$^{-/-}$ embryos showed complete absence of enteric neurons between the two smooth muscle layers (Fig. 7F). This was further confirmed by the lack of peripherin staining (Fig. 7F, inset). In order to analyze how enteric neuroblasts colonize the developing gut, we crossed *ECE-1*$^{+/-}$ mice to *DβH-nlacZ* transgenic mice. It was shown previously that migrating enteric neuroblasts transiently express *DβH* during development. The *DβH* promoter/enhancer region faithfully replicates this spatiotemporal expression pattern of the endogenous *DβH* gene when used to drive transgene expression (Kapur et al., 1991). Transgenic expression in enteric neuroblasts starts at E9.5 from the proximal foregut and extends caudally, such that the entire length of the gastrointestinal tract contain *nlacZ*-positive cells by E13.5. We used this *DβH-nlacZ* transgene to visualize migrating enteric neuroblasts in vivo. Males that were heterozygous for *ECE-1* and homozygous for *DβH-nlacZ* transgene were generated and bred to *ECE-1*$^{+/-}$ females. Pregnant females were killed at E12.0, and *ECE-1*$^{+/+}$, *ECE-1*$^{+/-}$ and *ECE-1*$^{-/-}$ embryos that were positive for the transgene were obtained. The entire gut was dissected and examined morphologically. There was no difference in the size of the gut between homozygous embryos and wild-type littermates. Whole-mount X-gal staining of the gut from wild-type embryos showed *nlacZ*-positive enteric neurons well into the large

Table 1. Genotype of embryos from $ET_A^{+/-}$; $ET_B^{+/-}$ double heterozygous crosses at E13.5

ET_B genotype	ET_A genotype +/+	+/–	–/–	Total
+/+	3 (0)*	9 (0)	2 (2)	14 (0)
+/–	10 (0)	15 (0)	8 (4)	33 (4)
–/–	5 (1)	8 (2)	0 (3)	13 (6)
Total	18 (1)	32 (2)	10 (7)	60 (10)

*The number of dead embryos assessed by gross observation in parenthesis.

intestine (Fig. 7G). In contrast, *nlacZ*-positive enteric neurons were only seen in the proximal gut in *ECE-1*$^{-/-}$ embryos, and they were absent beyond the ileocecal junction (Fig. 7H). This clearly showed that vagal neural crest cells were able to enter the developing gut, differentiate into the neuronal lineage and start migrating caudally. However, complete colonization of the gut by neuroblasts was impaired in the absence of ECE-1.

Double homozygous ET_A/ET_B-deficient embryos die in mid-gestation

We have shown that disruption of *ECE-1* impaired the production of both ET-1 and ET-3. It is tempting to speculate that this would completely abolish the local signals mediated by both ET_A and ET_B receptors, leading to the embryonic lethality. To test this hypothesis, we intercrossed double heterozygous $ET_A^{+/-}$; $ET_B^{+/-}$ mice on an inbred 129SvEv background (Hosoda et al., 1994; Clouthier et al., 1998) and examined 70 resulting embryos at E13.5 (see Table 1). $ET_A^{-/-}$; $ET_B^{+/-}$ embryos showed 33% lethality (4/12) and $ET_A^{+/-}$; $ET_B^{-/-}$ embryos showed 20% lethality (2/10). Other embryos, including $ET_A^{+/-}$; $ET_B^{+/-}$ embryos, were viable except one $ET_A^{+/+}$; $ET_B^{-/-}$ embryo that was dead in utero. However, all $ET_A^{-/-}$; $ET_B^{-/-}$ embryos obtained showed pericardial effusion and marked dilatation of peripheral vessels, and had died apparently from cardiac failure, highly resembling *ECE-1*$^{-/-}$ embryos (3/3, see Fig. 4B). These results support the idea that there is redundancy between ET_A and ET_B receptor-mediated signals involved in normal heart development.

DISCUSSION

ECE-1 is essential for proteolytic activation of both big ET-1 and big ET-3

The present study provides genetic evidence that ECE-1 is a physiologically relevant endothelin converting enzyme for both big ET-1 and big ET-3 in vivo. *ECE-1*$^{-/-}$ mice reproduced the phenotype resulting from the defects in both ET-1/ET_A- and ET-3/ET_B-mediated signaling pathways, which clearly shows that mature ET-1 and mature ET-3 are not synthesized in the relevant locations without ECE-1 activity. Consequently, there are no available ligands that can bind to ET_A and ET_B receptors to elicit biological effects. As a result, four distinct sets of neural crest derivatives, i.e., craniofacial structures, great vessels and conotruncal regions, enteric neurons, and epidermal and choroidal melanocytes are disrupted in *ECE-1*$^{-/-}$ mice.

A bulk of the mesenchyme of the head and neck is derived from the cephalic neural crest. As the neural tube closes, cephalic neural crest cells undergo an epithelial-mesenchymal transition and migrate ventrolaterally to colonize the head and branchial arches. The most severely affected craniofacial structures in *ECE-1*$^{-/-}$ mice are the mandible and associated ducts and glands, the hyoid, Meckel's cartilage, the tympanic ring and the middle ear ossicles. They are derivatives of the first and second branchial arches where neural crest cells from the level of the posterior midbrain and hindbrain colonize (Köntges and Lumsden, 1996). This phenotype seen in *ECE-1*$^{-/-}$ mice is virtually identical to *ET-1*$^{-/-}$ and $ET_A^{-/-}$ mice, which strongly suggest that big ET-1 cannot be cleaved to produce biologically active mature ET-1 without ECE-1 activity, thus impairing ET-1/ET_A-mediated signaling in *ECE-*

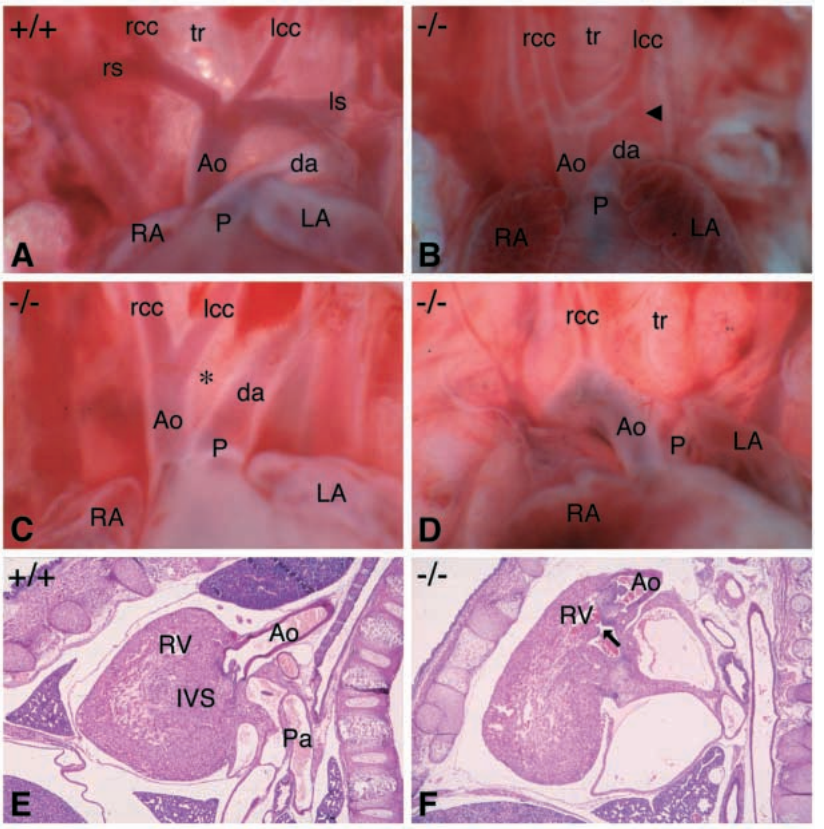

Fig. 6. Cardiovascular defects in E18.5 *ECE-1*$^{-/-}$ and wild-type embryos. (A-D) Gross photographs of the heart and great vessels. *ECE-1* genotype is indicated in each panel. (B) Tubular hypoplasia of the aortic arch (arrowhead). (C) Interruption of the aortic arch (*) and absence of the right subclavian artery (rs). The left subclavian artery is present but obstructed from view. (D) Right-sided aortic arch. (E,F) Parasagittal sections of the heart stained with hematoxylin and eosin. (F) The aorta overrides the perimembranous VSD (arrow). da, ductus arteriosus; ivs, interventricular septum; lcc, left common carotid artery; ls, left subclavian artery; P, pulmonary trunk; Pa, pulmonary artery; rcc, right common carotid artery; tr, trachea.

1$^{-/-}$ mice. This observation also confirms that ET-1/ET_A-mediated signaling is critical for proper development of neural crest derivatives in the branchial arches.

The mechanism in which ET-1/ET_A-mediated intercellular signaling is involved in cephalic neural crest development is not completely understood. ET-1 may be necessary for migration, proliferation or differentiation of neural crest cells. In branchial arches, *ET-1* mRNA is expressed in the surface epithelium and paraxial mesoderm core, while *ET_A* mRNA is expressed in migrating neural crest cells and in the mesenchyme of the branchial arches (Clouthier et al., 1998). Interestingly, *ECE-1* mRNA is expressed in both surface epithelium and mesenchyme of the branchial arches as well as in head mesenchyme. It was previously reported that cephalic neural crest cells and paraxial mesoderm cells are spatially segregated in the branchial arches and yet are both required to elaborate the mesenchymal patterning (Trainor and Tam, 1995). It is intriguing to postulate that ECE-1 contributes to the local production of mature ET-1 in the branchial arch epithelium and the paraxial mesoderm core of the arches, as well as to the conversion of secreted big ET-1 extracellularly on the surface of the ET_A-positive neural crest cells. ECE-1 therefore enables the activation of the ET_A receptor by mature ET-1, which is essential for the epithelial-mesenchymal interaction involved in branchial arch development.

The cardiac abnormalities seen in *ECE-1*$^{-/-}$ mice are mainly defects in patterning of great vessels and conotruncal regions. Type B interrupted aortic arch (Van Mierop and Kutsche, 1984), which results from disturbance of the left fourth aortic arch development, is most commonly observed. Among the conotruncal disorders, a perimembranous VSD is seen in all cases and dextroposed aorta (including both DORV and overriding of aorta) is frequently observed. Neural crest cells in brachial arches 3, 4 and 6 are known to migrate and contribute to the formation of outflow tract septation and conotruncal regions (Kirby and Waldo, 1995). It was shown previously that removal of a large amount of cardiac neural crest resulted in PTA while removal of a small amount of cardiac neural crest resulted in a variety of defects that include dextroposed aorta (Nishibatake et al., 1987). The frequency of PTA in *ECE-1*$^{-/-}$ or *ET_A*$^{-/-}$ embryos is relatively low compared with *Splotch* mutants (Franz, 1993) and NF-1 knockout mice (Brannan et al., 1994). It is also known that initial migration of cardiac neural crest cells is impaired in the *Splotch* mutation (Conway et al., 1997). Overall, however, the cardiac phenotype in *ECE-1*$^{-/-}$ embryos highly resembles those observed in neural crest-ablated chicken embryos (Nishibatake et al., 1987), neurotrophin-3 knockout mice (Donovan et al., 1996), RAR α and β_2 double knockout mice (Mendelsohn et al., 1994), activin type IIB receptor knockout mice (Oh and Li, 1997), as well as the CATCH 22 syndrome in humans (Wilson et al., 1993), all of which have defects in neural crest development. ET-1/ET_A-mediated signaling may act in a final environment to promote proliferation or differentiation of neural crest cells, rather than affecting their migration.

It was shown previously that ECE-1 cleaves big ET-1 more

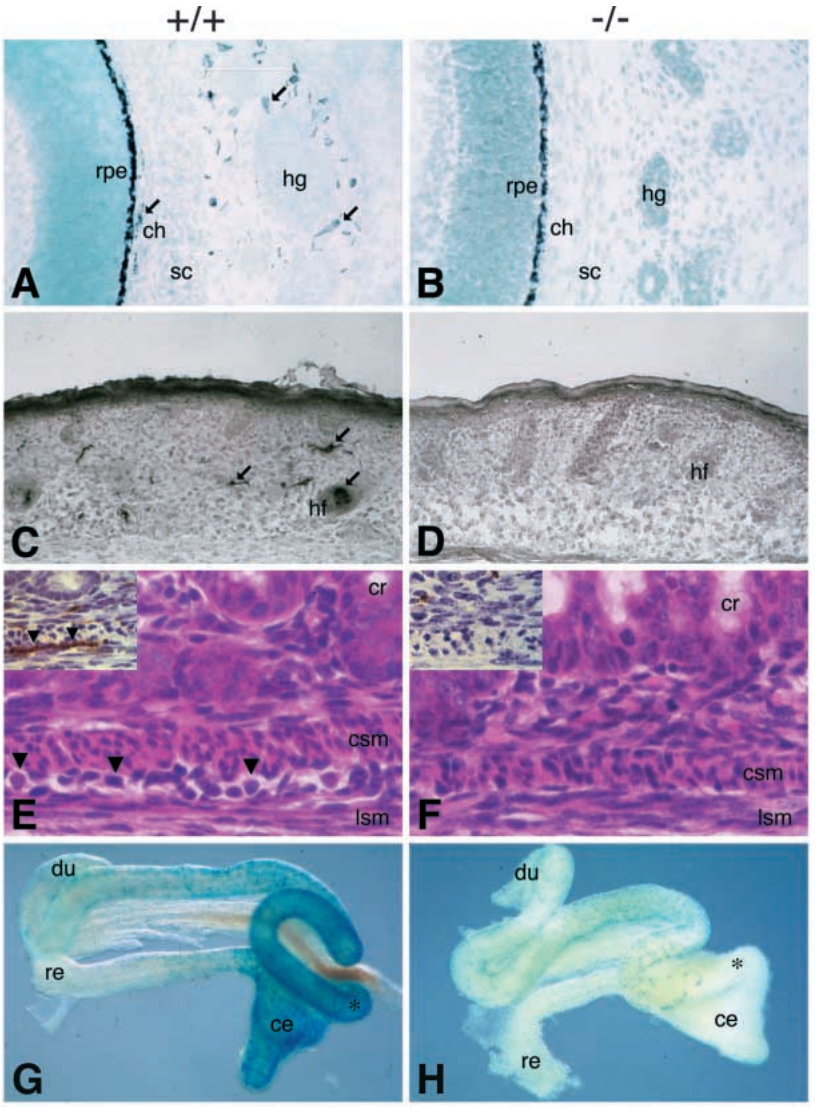

Fig. 7. Examination of melanocytes and enteric neurons in P0 mice (A-D), E18.5 embryos (E,F), and E12.0 embryos (G-H). Left panels, wild-type; right panels, *ECE-1*$^{-/-}$. (A,B) Frozen sections of the head stained with methyl green. Neural crest-derived choroidal (ch) and Harderian gland (hg) melanocytes (arrows) are absent in *ECE-1*$^{-/-}$ embryo (B). (C,D) L-DOPA histochemistry on frozen sections of dorsal skin. Interfollicular and follicular melanocytes (arrows) are absent in *ECE-1*$^{-/-}$ embryo (D). (E,F) Sagittal sections of rectum stained with hematoxylin and eosin as well as with anti-peripherin antibodies (insets). Note that enteric neurons (arrowheads in E) between the circular smooth muscle layer (csm) and longitudinal smooth muscle layer (lsm) are absent in *ECE-1*$^{-/-}$ embryo (F). (G, H) Whole-mount X-gal staining of the gut from *ECE-1*$^{+/+}$*; DβH-nlacZ* (G) and *ECE-1*$^{-/-}$*; DβH-nlacZ* (H) embryos. Note that X-gal-positive enteric neurons are absent beyond the ileocecal junction (*) in the mutant (H). ce, cecum; cr, crypt; du, duodenum; hf, hair follicle; re, rectum; rpe, retinal pigmented epithelium; sc, sclera.

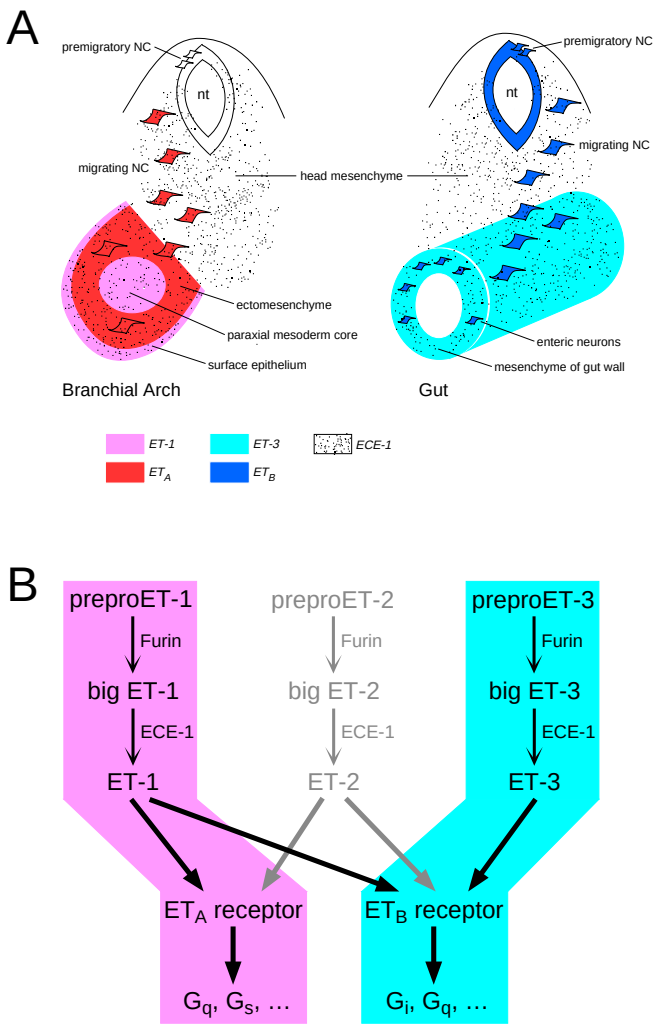

Fig. 8. (A) Expression patterns of endothelin-related molecules in the branchial arch and gut. *ET-1* mRNA is expressed in the surface epithelium and paraxial mesodermal core of the branchial arches, while ET_A mRNA is observed in migrating cephalic neural crest cells (NC) and neural crest-derived ectomesenchymal cells of the arches. *ET-3* mRNA occurs in the mesenchyme of the gut, while ET_B mRNA is expressed by enteric neurons derived from the vagal neural crest. Note that the neuroepithelium and both premigratory and migrating crest cells express ET_B mRNA, whereas ET_A mRNA is not expressed by premigratory crest cells. *ECE-1* mRNA is expressed in surface epithelium, ectomesenchyme and the paraxial mesoderm core of the arches, as well as head and gut mesenchyme. Similar endothelin-mediated interactions involving the neural crest and surrounding cells are observed during development of the cardiac outflow tract and epidermal melanoblasts (see text). nt, neural tube. (B) Endothelin pathways. Big endothelins are first produced from the three prepro-precursors through proteolytic processing catalized by furin or similar serin protease(s). ECE-1 and ECE-2 are two known membrane-bound metalloproteases that can cleave the biologically inactive big endothelins into the 21-amino-acid, active endothelins. Mature endothelins act on the two known G protein-coupled endothelin receptors. Red represents the ET-1/ECE-1/ET_A pathway involved in development of neural crest derivatives in branchial arches and cardiac outflow tissues. Blue represents the ET-3/ECE-1/ET_B pathway that regulates development of melanocytes and enteric neurons.

effectively among the three isopeptides. It was therefore important to examine whether any phenotype resulting from the defect in cleavage of big ET-2 or big ET-3 developed in *ECE-1*$^{-/-}$ embryos. *ECE-1*$^{-/-}$ embryos showed an absence of choroidal melanocytes, Harderian gland melanocytes and epidermal melanocytes, all of which are derivatives of cephalic and trunk neural crest. They also lacked enteric neurons in the distal colon, completely reproducing the phenotype observed in *ET-3*$^{-/-}$ and *ET*$_B^{-/-}$ embryos. *ECE-1* mRNA is expressed in the mesenchyme of the gut and the dermis, where interaction of ET-3 and ET_B takes place (R. P. Kapur et al., unpublished data). In addition, mature ET-3 levels in near-term embryos determined by EIA were dramatically decreased in *ECE-1*$^{-/-}$ embryos. Taken together, these data provide genetic and biochemical evidence that ECE-1 is a relevant cleaving enzyme for big ET-3 in vivo. Whether ECE-1 cleaves big ET-2 in vivo remains unclear. Since *ET-2* mRNA is expressed exclusively in the postnatal gastrointestinal tract in mice (our unpublished observation), the potential phenotype resulting from impaired cleavage of big ET-2 may not be observed in *ECE-1*$^{-/-}$ mice due to neonatal lethality.

The X-gal staining of the gut of E12.0 *DβH-nlacZ* transgenic *ECE-1*$^{-/-}$ embryos showed that enteric neuroblasts had colonized only the proximal gut in contrast to wild-type embryos, which showed enteric neurons in distal gut. It has been shown that *ET*$_B$ mRNA is expressed in migrating enteric neuroblasts and *ET-3* mRNA is expressed in the mesenchyme of the gut (R. P. Kapur et al., unpublished data). Mature ET-3 cannot be produced in gut mesenchyme without ECE-1 activity, and therefore ET-3/ET_B-mediated signaling is absent in *ECE-1*$^{-/-}$ embryos. A similar phenotype resulting in aganglionic megacolon was reported in mice deficient for *GDNF* and its receptor *RET*. Interestingly, *RET* mRNA is expressed in enteric neuroblasts while *GDNF* mRNA is expressed in surrounding mesenchyme of the gut (Pachnis et al., 1993; Hellmich et al., 1996). In *GDNF*$^{-/-}$ and *RET*$^{-/-}$ embryos, migrating enteric neuroblasts in the foregut failed to colonize the entire midgut and hindgut (Schuchardt et al., 1994; Moore et al., 1996; Pichel et al., 1996; Sánchez et al., 1996). The length of aganglionosis in these mice was much greater than that of *ET-3*$^{-/-}$, *ET*$_B^{-/-}$ or *ECE-1*$^{-/-}$ embryos. However, it is clear that reciprocal signaling between enteric neurons and surrounding mesenchyme including ET-3/ET_B and GDNF/RET pathways are necessary for proper colonization of enteric neuroblasts in the distal gut. It remains to be elucidated whether ET-3/ET_B and GDNF/RET pathways exist in parallel and affect different populations of enteric neuroblasts or whether they work synergistically to maintain the proliferating capacity of enteric neuroblasts required for caudal progression.

ET-1 functions only locally whereas big ET-1 can act as a distant carrier of ET-1 signals

Tissue peptide analyses showed that a significant amount of mature ET-1/ET-2 still existed in *ECE-1*$^{-/-}$ embryos despite the absence of ECE-1 enzyme activity. This strongly suggests that other peptidase(s), such as ECE-2 (Emoto and Yanagisawa, 1995), are present in near-term embryos and are responsible for the production of mature endothelins in *ECE-1*$^{-/-}$ embryos. Importantly, however, these remaining mature endothelins completely failed to ‘rescue’ the developmental phenotype of

ECE-1$^{-/-}$ mice. This clearly demonstrates that mature endothelins must be produced at specific sites in order to influence development. Our series of endothelin-related gene disruption studies (Baynash et al., 1994; Hosoda et al., 1994; Clouthier et al., 1998), together with previous pharmacological findings (Yanagisawa, 1994), establish that mature ET-1 acts only locally. However, it is noteworthy that both *ECE-1*$^{-/-}$ and *ET*$_A^{-/-}$ embryos showed complete penetrance of cardiovascular abnormalities in contrast to *ET-1*$^{-/-}$ embryos, which showed a low incidence of the same defects (Kurihara et al., 1995). In order to produce the comparable cardiac phenotype with similar frequency, pregnant *ET-1*$^{+/-}$ females had to be administered either neutralizing antibodies to ET-1 or an ET_A-specific antagonist during the pregnancy. These discrepancies suggest that maternally or placentally derived big ET-1, but not mature ET-1, is delivered to the developing heart and locally converted to ET-1 by ECE-1, thus partially rescuing the cardiovascular phenotype in *ET-1*$^{-/-}$ embryos. This illustrates that big ET-1 can act as a long-distance carrier of the biological action of ET-1 in vivo.

Functional redundancy of ET_A and ET_B receptors in cardiac development

ECE-1$^{-/-}$ embryos showed embryonic lethality apparently due to cardiac failure, which was not observed in any of the single knockouts of endothelin-related molecules, i.e., ET-1, ET-2, ET-3, ET_A, ET_B and ECE-2. The unique role of ECE-1 in cardiac development may be due in part to its ability to cleave both big ET-1 and big ET-3 in vivo. The double homozygous mutants for *ET*$_A$ and *ET*$_B$ exhibit an embryonic lethal phenotype highly similar to *ECE-1*$^{-/-}$ embryos, and the expression of both receptor genes is observed in the heart. This suggests that there is functional redundancy between *ET*$_A$ and *ET*$_B$ in cardiac development. Alternatively, ECE-1 may cleave non-endothelin-related peptides necessary for normal cardiac development, especially peptides involved in endocardial cushion development, such as neuregulin and their receptors (Gassmann et al., 1995; Lee et al., 1995; Meyer and Birchmeier, 1995).

ECE-1 integrates the dual axes of endothelin-mediated signaling essential for the development of specific subsets of neural crest-derived tissues

Null mutation of *ECE-1* affects the development of four distinct groups of tissues, all of which are derived from subpopulations of neural crest cells: the branchial arch-derived craniofacial tissues, great vessel and cardiac outflow structures, epidermal and choroidal melanocytes, and enteric neurons. This study, together with our additional findings (Baynash et al., 1994; Hosoda et al., 1994; Clouthier et al., 1998), establishes the two axes of endothelin-mediated signaling in embryonic development, i.e., the ET-1/ECE-1/ET_A and ET-3/ECE-1/ET_B pathways (Fig. 8). These two signaling pathways act independently in development of subsets of neural crest lineages and ECE-1 plays a central role in these endothelin-mediated signaling pathways. Along with $G\alpha_{13}$ (Offermanns et al., 1997) and the 5-HT2B receptor (Choi et al., 1997), these pathways represent important examples of heterotrimeric G protein-coupled signaling mechanisms essential for vertebrate development.

We thank Shan Maika, Lucy Lindquist, Beth Hinnant, John Shelton, Robert Webb and Jian Xie for technical assistance, Allan Bradley for LIF-producing STO cells, Nobuhiro Suzuki for EIA antibodies, and Cheryl Gariepy, Joe Goldstein and Mike Brown for critical reading of the manuscript. M. Y. is an Investigator, and D. E. C. and N. E. are Associates of the Howard Hughes Medical Institute. This study is supported in part by research grants from the Perot Family Foundation, Excellence in Education Fund, and the W. M. Keck Foundation.

REFERENCES

Arai, H., Hori, S., Aramori, I., Ohkubo, H. and Nakanishi, S. (1990). Cloning and expression of a cDNA encoding an endothelin receptor. *Nature* **348,** 730-732.

Baynash, A. G., Hosoda, K., Giaid, A., Richardson, J. A., Emoto, N., Hammer, R. E. and Yanagisawa, M. (1994). Interaction of endothelin-3 with endothelin-B receptor is essential for development of epidermal melanocytes and enteric neurons. *Cell* **79,** 1277-1285.

Benjamin, I. J., Shelton, J., Garry, D. J. and Richardson, J. A. (1997). Temporospatial expression of the small HSP/αB-crystallin in cardiac and skeletal muscle during mouse development. *Dev. Dyn.* **208,** 75-84.

Brannan, C. I., Perkins, A. S., Vogal, K. S., Ratner, N., Nordlund, M. L., Reid, S. W., Buchberg, A. M., Jenkins, N. A., Parada, L. F. and Copeland, N. G. (1994). Targeted disruption of the neurofibromatosis type-1 gene leads to developmental abnormalities in heart and various neural crest-derived tissues. *Gene Dev.* **8,** 1019-1029.

Choi, D.-S., Ward, S. J., Messaddeq, N., Launay, J.-M. and Maroteaux, L. (1997). 5-HT2B receptor-mediated serotonin morphogenetic functions in mouse cranial neural crest and myocardiac cells. *Development* **124,** 1745-1755.

Conway, S. J., Henderson, D. J. and Copp, A. J. (1997). *Pax3* is required for cardiac neural crest migration in the mouse: evidence from the *sploth* (*SP*^{2h}) mutant. *Development* **124,** 505-514.

Clouthier, D. E., Hosoda, K., Richardson, J. A. Williams, S. C., Yanagisawa, H., Kuwaki, T., Kumada, M., Hammer, R. E. and Yanagisawa, M. (1998). Cranial and cardiac neural crest defects in endothelin-A receptor-deficient mice. *Development* **125**, 813-824.

Donovan, M. J., Hahn, R., Tessarollo, L. and Hempstead, B. L. (1996). Identification of an essential nonneuronal function of neurotrophin 3 in mammalian cardiac development. *Nature Genet.* **14,** 210-213.

Durbec, P. L., Larsson-Blumberg, L. B., Schuchardt, A., Constantini, F. and Pachnis, V. (1996). Common origin and developmental dependence on c-ret of subsets of enteric and sympathetic neuroblasts. *Development* **122,** 349-358.

Edery, P., Attie, T., Amiel, J., Pelet, A., Eng, C., Hofstra, R. M. W., Martelli, H., Bidaud, C., Munnich, A. and Lyonnet, S. (1996). Mutation of the endothelin-3 gene in the Waardenburg-Hirschsprung disease (Shah-Waardenburg syndrome). *Nature Genet.* **12,** 442-444.

Emoto, N. and Yanagisawa, M. (1995). Endothelin-converting enzyme-2 is a membrane-bound, phosphoramidon-sensitive metalloprotease with acidic pH optimum. *J. Biol. Chem.* **270,** 15262-15268.

Epstein, M. L., Mikawa, T., Brown, A. M. C. and McFarlin, D. R. (1994). Mapping the origin of the avian enteric nervous system with a retroviral marker. *Dev. Dyn.* **201,** 236-244.

Erickson, C. A. (1993). From the crest to the periphery: control of pigment cell migration and lineage segregation. *Pigment Cell Res.* **6,** 336-347.

Franz, T. (1993). The Splotch (Sp^{1H}) and Splotch-delayed (Sp^{d}) alleles: differential phenotypic effects on neural crest and limb musculature. *Anat. Embryol.* **187,** 371-377.

Gassmann, M., Casagranda, F., Orioli, D., Simon, H., Lai, C., Klein, R. and Lemke, G. (1995). Aberrant neural and cardiac development in mice lacking the ErbB4 neuregulin receptor. *Nature* **378,** 390-394.

Hellmich, H. L., Kos, L., Cho, E. S., Mahon, K. A. and Zimmer, A. (1996). Embryonic expression of glial cell-line derived neurotrophic factor (GDNF) suggests multiple developmental roles in neural differentiation and epithelial-mesenchymal interactions. *Mech. Dev.* **54,** 95-105.

Hofstra, R. M. W., Osinga, J., Tan-Sindhunata, G., Wu, Y., Kamsteeg, E.-J., Stulp, R. P., Ravenswaaij-Arts, C. V., Majoor-Krakauer, D., Angrist, M., Chakravarti, A., Meijers, C. and Buys, C. H. C. M. (1996). A homozygous mutation in the endothelin-3 gene associated with a combined Waardenburg type 2 and Hirschsprung phenotype (Shah-Waardenburg syndrome). *Nature Genet.* **12,** 445-447.

Hosoda, K., Hammer, R. E., Richardson, J. A., Baynash, A. G., Cheung, J. C., Giaid, A. and Yanagisawa, M. (1994). Targeted and natural (piebald-

lethal) mutations of endothelin-B receptor gene produce megacolon associated with spotted coat color in mice. *Cell* **79,** 1267-1276.

Inoue, A., Yanagisawa, M., Kimura, S., Kasuya, Y., Miyauchi, T., Goto, K. and Masaki, T. (1989). The human endothelin family: Three structurally and pharmacologically distinct isopeptides predicted by three separate genes. *Proc. Natl. Acad. Sci. USA* **86,** 2863-2867.

Ishibashi, S., Brown, M. S., Goldstein, J. L., Gerard, R. D., Hammer, R. E. and Herz, J. (1993). Hypercholesterolemia in low density lipoprotein receptor knockout mice and its reversal by adenovirus-mediated gene delivery. *J. Clin. Invest.* **92,** 883-893.

Kapur, R. P., Hoyle, G. W., Mercer, E. H., Brinster, R. L. and Palmiter, R. D. (1991). Some neuronal cell populations express human dopamine β-hydroxylase-*lacZ* transgenes transiently during embryonic development. *Neuron* **7,** 717-727.

Kirby, M. L., Gale, T. F. and Stewart, D. E. (1983). Neural crest cells contribute to normal aorticopulmonary septation. *Science* **220,** 1059-1061.

Kirby, M. L. and Waldo, K. L. (1995). Neural crest and cardiovascular patterning. *Circ. Res.* **77,** 211-215.

Kochhar, D. M. (1973). Limb development in mouse embryos. I. Analysis of teratogenic effects of retinoic acid. *Teratology* **7,** 289-298.

Köntges, G. and Lumsden, A. (1996). Rhombencephalic neural crest segmentation is preserved throughout craniofacial ontogeny. *Development* **122,** 3229-3242.

Kuratani, S. C. and Kirby, M. L. (1991). Initial migration and distribution of the cardiac neural crest in the avian embryo: an introduction to the concept of the circumpharyngeal crest. *Am. J. Anat.* **191,** 215-227.

Kurihara, Y., Kurihara, H., Oda, H., Maemura, K., Nagai, R., Ishikawa, T. and Yazaki, Y. (1995). Aortic arch malformations and ventricular septal defect in mice deficient in endothelin-1. *J. Clin. Invest.* **96,** 293-300.

Kurihara, Y., Kurihara, H., Suzuki, H., Kodama, T., Maemura, K., Nagai, R., Oda, H., Kuwaki, T., Cao, W.-H., Kamada, N., Jishage, K., Ouchi, Y., Azuma, S., Toyoda, Y., Ishikawa, T., Kumada, M. and Yazaki, Y. (1994). Elevated blood pressure and craniofacial abnormalities in mice deficient in endothelin-1. *Nature* **368,** 703-710.

Le Douarin, N. M., Dupin, E. and Ziller, C. (1994). Genetic and epigenetic control in neural crest development. *Curr. Opin. Genet. Dev.* **4,** 685-695.

Le Douarin, N. M., Ziller, C. and Couly, G. F. (1993). Patterning of neural crest derivatives in the avian embryo: In vivo and in vitro studies. *Dev. Biol.* **159,** 24-49.

Le Lièvre, C. S. and Le Douarin, N. M. (1975). Mesenchymal derivatives of the neural crest: analysis of chimaeric quail and chick embryos. *J. Embryol. Exp. Morph.* **34,** 125-154.

Lee, K.-F., Simon, H., Chen, H., Bates, B., Hung, M.-C. and Hauser, C. (1995). Requirement for neuregulin receptor erbB2 in neural and cardiac development. *Nature* **378,** 394-398.

Loring, J. F. and Erickson, C. A. (1987). Neural crest cell migratory pathways in the trunk of the chick embryo. *Dev. Biol.* **121,** 220-236.

Maemura, K., Kurihara, H., Kurihara, Y., Oda, H., Ishikawa, T., Copeland, N. G., Gilbert, D. J., Jenkins, N. A. and Yazaki, Y. (1996). Sequence analysis, chromosomal location, and developmental expression of the mouse preproendothelin-1 gene. *Genomics* **31,** 177-184.

Matsumoto, H., Suzuki, N., Onda, H. and Fujino, M. (1989). Abundance of endothelin-3 in rat intestine, pituitary glands and brain. *Biochem. Biophys. Res. Commun.* **164,** 74-80.

Mendelsohn, C., Lohnes, D., Décimo, D., Lufkin, T., LeMeur, M., Chambon, P. and Mark, M. (1994). Function of the retinoic acid receptors (RARs) during development(II). Multiple abnormalities at various stages of organogenesis in RAR double mutants. *Development* **120,** 2749-2771.

Meyer, D. and Birchmeier, C. (1995). Mutiple essential functions of neuregulin in development. *Nature* **378,** 386-390.

Moore, M. W., Klein, R. D., Fariñas, I., Sauer, H., Armanini, M., Phillips, H., Reichardt, L. F., Ryan, A. M., Carver-Moore, K. and Rosenthal, A. (1996). Renal and neuronal abnormalities in mice lacking GDNF. *Nature* **382,** 76-79.

Nishibatake, M., Kirby, M. L. and Van Mierop, L. H. S. (1987). Pathogenesis of persistent truncus arteriosus and dextroposed aorta in the chick embryo after neural crest ablation. *Circulation* **75,** 255-264.

Noden, D. M., Poelmann, R. E. and Gittenberger-de Groot, A. C. (1995). Cell origins and tissue boundaries during outflow tract development. *Trends Cardiovasc. Med.* **5,** 69-75.

Offermanns, S., Mancino, V., Revel, J.-P. and Simon, M. I. (1997). Vascular system defects and impaired cell chemokinesis as a result of $G\alpha_{13}$ deficiency. *Science* **275,** 533-536.

Oh, S. P. and Li, E. (1997). The signaling pathway mediated by the type IIB activin receptor controls axial patterning and lateral asymmetry in the mouse. *Gene Dev.* **11,** 1812-1826.

Pachnis, V., Mankoo, B. and Costantini, F. (1993). Expression of the c-ret proto-oncogene during mouse embryogenesis. *Development* **119,** 1005-1017.

Pichel, J. G., Shen, L., Sheng, H. Z., Granholm, A.-C., Drago, J., Grinberg, A., Lee, E. J., Huang, S. P., Saarma, M., Hoffer, B. J., Sariola, H. and Westphal, H. (1996). Defects in enteric innervation and kidney development in mice lacking GDNF. *Nature* **382,** 73-76.

Puffenberger, E. G., Hosoda, K., Washington, S. S., Nakao, K., deWit, D., Yanagisawa, M. and Chakravarti, A. (1994). A missense mutation of the endothelin-B receptor gene in multigenic Hirschsprung disease. *Cell* **79,** 1257-1266.

Rawlings, N. D. and Barrett, A. J. (1993). Evolutionary families of peptidases. *Biochem. J.* **290,** 205-218.

Rodriguez, H. A. and McGavran, M. H. (1969). A modified dopa reaction for the diagnosis and investigation of pigment cells. *Am. J. Clin. Pathol.* **52,** 219-227.

Sakurai, T., Yanagisawa, M., Takuwa, Y., Miyazaki, H., Kimura, S., Goto, K. and Masaski, T. (1990). Cloning of a cDNA encoding a non-isopeptide-selective subtype of the endothelin receptor. *Nature* **348,** 732-735.

Sánchez, M. P., Silos-Santiago, I., Frisén, J., He, B., Lira, S. A. and Barbacid, M. (1996). Renal agenesis and the absence of enteric neurons in mice lacking GDNF. *Nature* **382,** 70-73.

Schuchardt, A., D'Agati, V., Larsson-Blomberg, L., Costantini, F. and Pachnis, V. (1994). Defects in the kidney and enteric nervous system of mice lacking the tyrosine kinase receptor Ret. *Nature* **367,** 380-383.

Serbedzija, G. N., Bronner-Fraser, M. and Fraser, S. E. (1992). Vital dye analysis of cranial neural crest cell migration in the mouse embryo. *Development* **116,** 297-307.

Serbedzija, G. N. and McMahon, A. P. (1997). Analysis of neural crest cell migration in Splotch mice using a neural crest-specific lacZ reporter. *Dev. Biol.* **185,** 139-147.

Shah, N. M., Groves, A. K. and Anderson, D. J. (1996). Alternative neural crest cell fates are instructively promoted by TGFβ superfamily members. *Cell* **85,** 331-343.

Stemple, D. L. and Anderson, D. J. (1993). Lineage diversification of the neural crest: in vitro investigations. *Dev. Biol.* **159,** 12-23.

Suzuki, N., Matsumoto, H., Kitada, C., Kimura, S., Miyauchi, T. and Fujino, M. (1990). A sandwich-type enzyme immunoassay to detect immunoreactive big-endothelin-1 in plasma. *J. Immunol. Meth.* **127,** 165-170.

Trainor, P. A. and Tam, P. P. L. (1995). Cranial paraxial mesoderm and neural crest cells of the mouse embryo: co-distribution in the craniofacial mesenchyme but distinct segregation in branchial arches. *Development* **121,** 2569-2582.

Van Mierop, L. H. S. and Kutsche, L. M. (1984). Interruption of the aortic arch and coarctation of the aorta: Pathogenetic relations. *Am. J. Cardiol.* **54,** 829-834.

Wilson, D. I., Burn, J., Scambler, P. and Goodship, J. (1993). DiGeorge syndrome: part of CATCH 22. *J. Med. Genet.* **30,** 852-856.

Xu, D., Emoto, N., Giaid, A., Slaughter, C. A., Kaw, S., de Wit, D. and Yanagisawa, M. (1994). ECE-1: A membrane-bound metalloprotease that catalyzes the proteolytic activation of big endothelin-1. *Cell* **78,** 473-485.

Yanagisawa, M. (1994). The endothelin system: A new target for therapeutic intervention. *Circulation* **89,** 1320-1322.